Concentration- and Solvent-dependent Electron Spin Resonance Signals and Dimer Formation of High-spin Iron(III) Porphyrins

By **Makato Chikira, Hideo Kon,* and Kevin M. Smith,** Laboratory of Chemical Physics, National Institute of Arthritis, Metabolism and Digestive Diseases, Bethesda MD 20205 and Department of Chemistry, University of California at Davis, Davis, CA 95616, U.S.A.

High-spin iron(III) porphyrins in frozen solutions show extra e.s.r. signals, in addition to the well known parallel (g = 2) and perpendicular (g = 6) absorption, which are remarkably sensitive to the concentration, solvent composition, pH, or the temperature. For example, two signals with g values around 3 and 11, respectively, are observed in moderately concentrated solutions of chloro(*meso*-nitro-octaethylporphyrinato)iron(III), in neutral and alkaline solutions of hemin when methanol is added, or in acidic solutions of tetrasodium phenylporphyrintetrasulphonatoferrate(III). The signals to higher field with g *ca.* 3 are interpreted as belonging to a dimeric species, on the basis of a simulation made by assuming a structure having two porphyrin planes arranged parallel. Another characteristic signal, which was observed in alkaline solutions of hemin or the tetrasodium ferrate, appears as a pair of shoulders with the g = 6 monomer peak in the middle. This type of signal is assigned to a dimer having a large Fe–Fe distance as well as skew angle. The effect of adding methanol, ethanol, or sucrose to the alkaline solutions of hemin, inducing further additional signals, and that of NaCl addition, which suppresses the overall intensity, are described and discussed in relation to previous studies by spectrophotometric and magnetic susceptibility measurements.

THE dimerization and polymerization of iron porphyrins in solution are well known,[1] and have been studied mostly by spectrophotometric methods,[2-7] combined with temperature-jump,[8] electrochemical,[9] or magnetic susceptibility measurements.[10-12] Recently, n.m.r. methods have been applied to obtain structural information on dimeric species of various porphyrins, zinc(II) [13-15] and iron(III) [16,17] complexes, but there have been few e.s.r. studies of dimer formation in iron(III) porphyrins, especially in the high-spin state.

In the past, the aggregation of ferrihemes was explained in terms of dimer units existing in the form of loosely bound micelles of variable particle size.[3,18] In more recent studies, which were mostly carried out in solutions at room temperature, the results have been shown to be consistent only with a dimerization process.[4,7]

Structures proposed for the dimeric species in general include the covalently bound μ-oxo-type, the dihydroxo-bridged form, and the π–π type, of which only the first has been chemically identified and spectroscopically characterized for iron(III) porphyrins.[6,9,11,19] The dihydroxo-bridged form [20,21] and the π–π type dimerization [13-15,22] have been found in other metal complexes but not in the high-spin iron(III) porphyrins.

Here we present the e.s.r. spectra of halogeno(*meso*-nitro-octaethylporphyrinato)iron(III) (halide = F, Cl, or Br) and the *meso*-dinitro-analogues in toluene, of hemin chloride, and of tetrasodium phenylporphyrintetrasulphonatoferrate(III) in aqueous solutions.† The signals are remarkably sensitive to the solute concentration, the solvent composition, pH, or the temperature. Iron porphyrin complexes have been the subject of numerous e.s.r. studies, but the type of signals described here have never been reported. Some of the signals can be explained in terms of dimeric models based upon the results of spectral simulations and other evidence.

† More systematically 2,3,7,8,12,13,17,18-octaethyl-5-nitroporphyrinato(2−)iron(III) halide, 2,7,13,17-tetramethyl-3,18-divinylporphyrin-8,12-dipropionatoiron(III) chloride, and tetrasodium 5,10,15,20-tetrakis(*p*-sulphophenyl)porphyrinato(6−)-ferrate.

EXPERIMENTAL

The *meso*-nitro- and *meso*-dinitro-octaethylporphyrins were prepared as described before.[23] The FeCl complexes of these ligands were prepared by using iron(II) sulphate.[24]

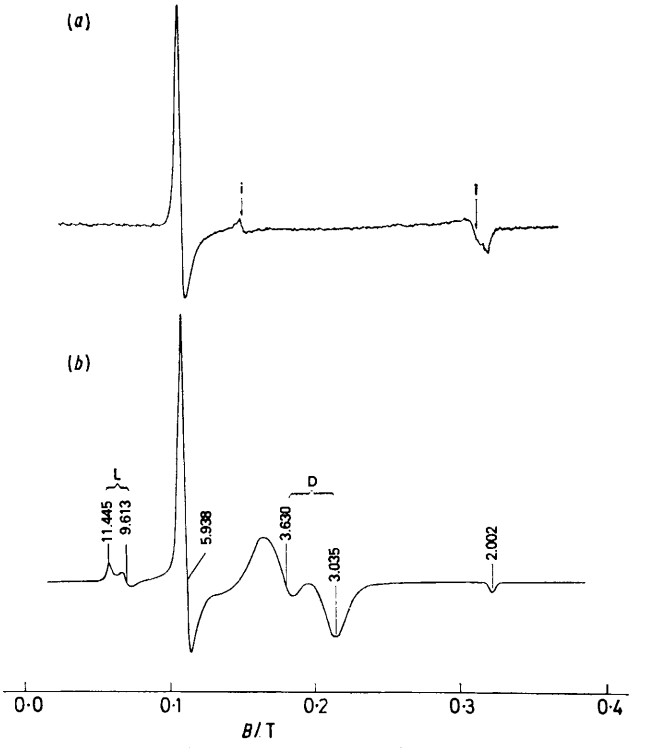

FIGURE 1 Comparison of e.s.r. spectra of compound (1) in frozen toluene solutions (14 K) at (*a*) 5.8 × 10^{-6} and (*b*) 1.87 × 10^{-3} mol dm^{-3}. The satellite signals D and L are not detectable in (*a*). The absorptions marked i are due to impurities

Fluoro- and bromo-analogues were obtained from the chloride by the method described in ref. 5. Hemin chloride (Sigma Chemical Co.) was used without further purification.

The porphyrintetrasulphonate salt was purchased from Man-Win Coordination Chemicals.

E.s.r. measurements were made in frozen solutions at 14 K, using a Varian E-9 *X*-band e.s.r. spectrometer with a 9-in magnet. The temperature was controlled by a Heli-Tran system (Air Products and Chemicals, Inc.). The microwave frequency was measured by a cavity wavemeter

perpendicular absorption of the high-spin iron(III) porphyrin monomer at $g = 6.0$, there are two new absorptions which are absent in dilute solution.[26] The one to higher field (denoted D) is a doublet with g values between 3 and 3.7 and is usually broader and more intense than the other doublet to lower field (L) with g around 10. As the total concentration of complex is decreased, both of these extra

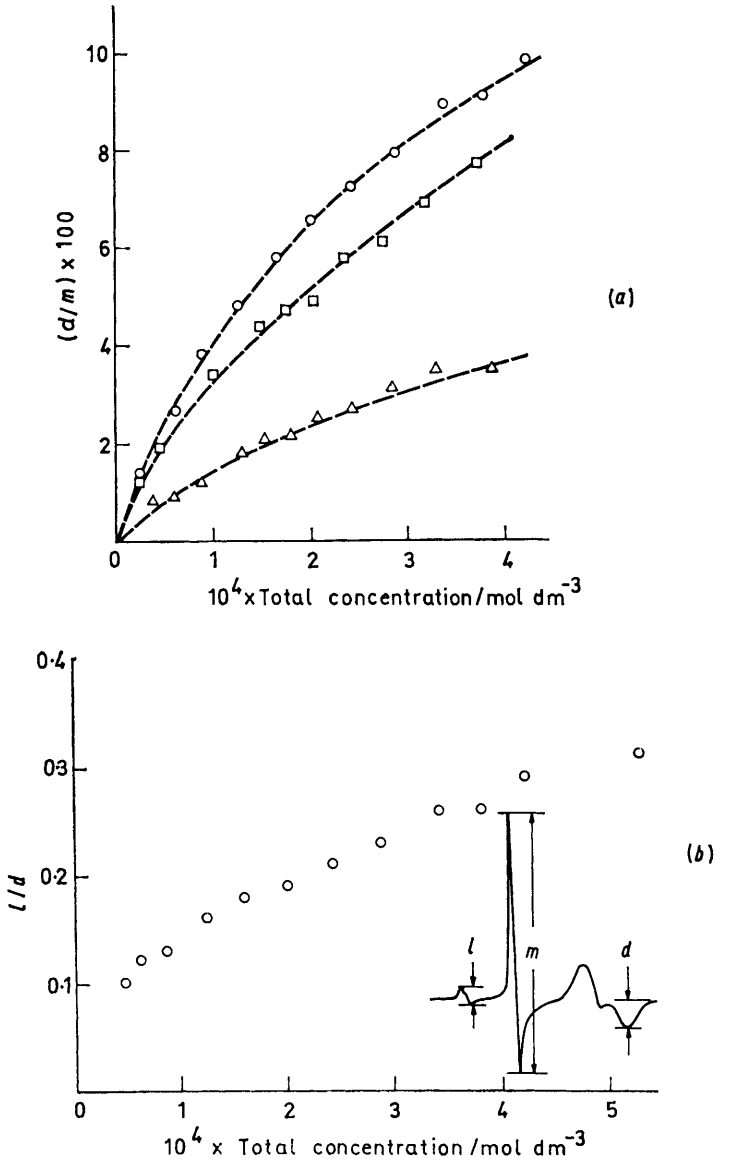

FIGURE 2 (*a*) E.s.r. intensity ratios of the signals shown in Figure 1. The measured heights are indicated in (*b*). Complexes: (○) [FeBr(noep)]: (□) [FeCl(noep)]; (△) [FeCl(oep)] where noep = *meso*-nitro-octaethylporphyrinate

calibrated at the National Bureau of Standards; the magnetic field was measured by using a ^1H n.m.r. probe.

The calculations and simulations of the dimer e.s.r. spectra were carried out by using the MLAB [25] program on a DEC-system 10.

RESULTS

E.S.R. Spectra in Toluene.—The e.s.r. spectrum of chloro-(*meso*-nitro-octaethylporphyrinato)iron(III) (1) in a frozen toluene solution at a concentration of 1.87×10^{-3} mol dm^{-3} is shown in Figure 1. In addition to the well known absorptions decrease in intensity and are almost undetectable at *ca.* 10^{-6} mol dm^{-3}. Such a concentration dependence is evidence that the extra signals are associated with dimerization and/or some higher-order association processes. The intensity ratios of the two signals are plotted [Figure 2(*b*)] as a function of the total concentration. Thus, as the concentration is decreased, the signal L decreases in intensity more than does the signal D. This behaviour suggests that the signal D is due to a dimer, while L may be due to some higher-order aggregation product. The intensity ratio of the satellites to that of the

monomer is affected by the type of solvent and the counter ion. The formation of the species giving rise to the satellites is more favoured in toluene than in a more polar solvent such as chloroform or dimethylformamide. As shown in Figure 2(*a*), the complex having Br^- as counter ion shows a higher intensity than that having Cl^-. The most remarkable increase in the satellite intensities is seen, however, as the result of *meso*-nitro- or α,β-*meso*-dinitro- (not shown) substitution(s) in the porphyrin ring, indicating the importance of electronic polarization for the formation of the association product. The g values and the line shapes are very similar in these complexes.

A complete change in the extra signals occurs when F^- is used as the counter ion. As shown in Figure 3, not only is the signal intensity relative to the $g = 6$ peak much smaller than in the Br^- or Cl^- analogue but also the peaks and troughs are farther apart from each other and they have approximately the same intensity on both sides of the $g = 6$ monomer absorption. The change in the intensity ratio is similar to that for other halides.

E.S.R. Spectra of Hemin in Aqueous Solutions.—Solutions were prepared by dissolving a calculated amount of hemin

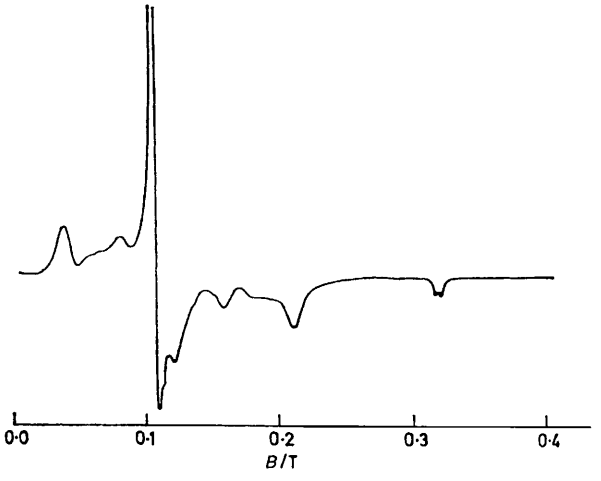

FIGURE 3 E.s.r. spectrum of [FeF(noep)] in a frozen toluene solution at 14 K and 5.2×10^{-4} mol dm^{-3}

in a small volume of aqueous K[OH] (1N) and diluting with distilled water. The pH was adjusted with aqueous HCl (1N).

At pH 6.2, the perpendicular peak of the high-spin hemin at $g = 6.10$ (measured at the peak position) is a single broad peak with extended tails, indicating that there is some aggregation and consequent spin-exchange interaction. In fact, at lower pH values, hemin starts to precipitate, and the spectrum may represent a small amount of crystalline material. As the pH is increased, the $g = 6.10$ signal becomes narrower and shows a line shape due to typical axial symmetry [Figure 4(*a*)]. The peak-to-trough height increases with pH, although there is no appreciable change in the total intensity up to pH *ca.* 8. Above this pH the peak-to-trough height begins to decrease, although the narrow, axial, line shape remains the same. At pH 10 a pair of shoulders develops roughly 0.013 T from the perpendicular peak on both sides as shown in Figure 4(*b*) for the case of pH 11.5. Increasing the pH further does not change the general line shape or the intensity. At this pH, dilution over the range 6×10^{-5}—10^{-3} mol dm^{-3} does not affect the shape or the relative intensity of the peaks.

When NaCl is added to this solution at concentrations of 0.5—2 mol dm^{-3} the resolution of the spectrum improves considerably, and, at the same time, the overall intensity decreases by roughly 50% [Figure 4(*c*)]. Simultaneously, a

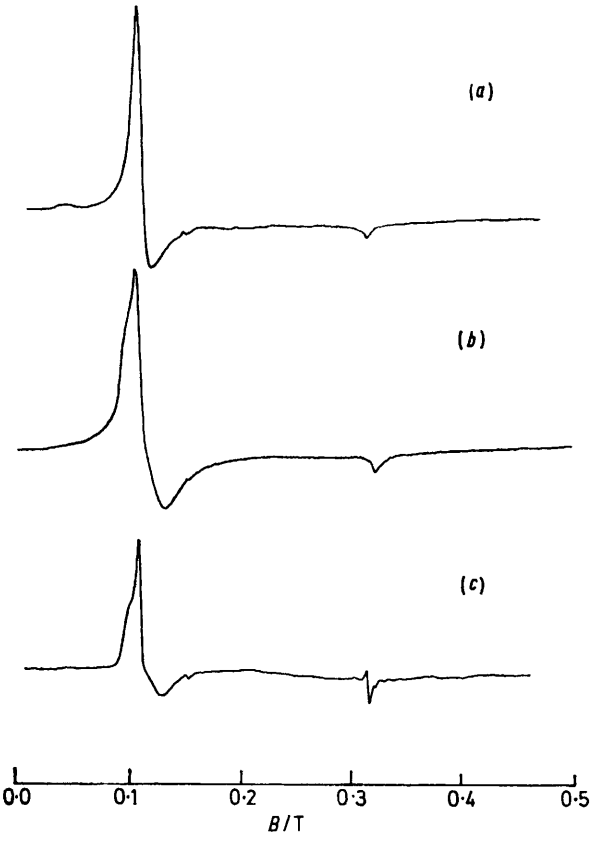

FIGURE 4 E.s.r. spectra of hemin in aqueous alkaline solutions at 14 K and 1×10^{-3} mol dm^{-3}. pH: (*a*) 7.7; (*b*) 11.5; (*c*) 11.5 with added NaCl (2 mol dm^{-3})

sharp peak appears at $g = 2.00$, which is likely to be due to a free-radical species. The intensity around $g = 6$ shows very little dependence on the NaCl concentration within the above range. The free-radical signal does not appear when the solution is prepared anaerobically, demonstrating

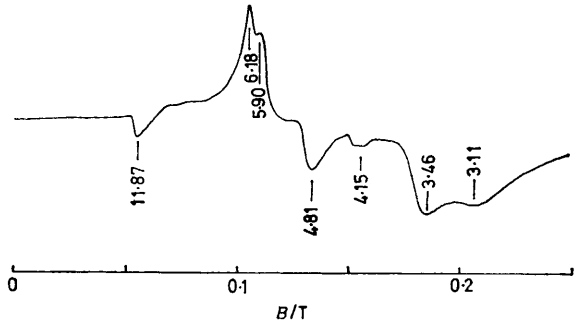

FIGURE 5 E.s.r. spectrum of hemin in aqueous solution (pH 7.1) with added methanol (1 : 4 v/v) at 14 K

that NaCl may somehow induce a chemical reaction involving molecular oxygen.

The addition of a small quantity of methanol ($\geqslant 4$ μl cm^{-3} or 0.1 mol dm^{-3}) to a hemin solution results in a dramatic change in the e.s.r. pattern. As shown in Figure 5, the

peaks around $g = 6$ lose some of their intensity and three new signals appear at $g = 6.18$, 5.90, and 4.81. The one at $g = 4.81$ decreases in intensity as the temperature is lowered, whereas the other two do not, showing that they originate from at least two different sources. Furthermore, when the hemin concentration is decreased, maintaining the same solvent composition, the peak at 6.18 increases and that at 5.90 decreases in intensity, indicating that these two are also different absorptions, and that the one at 6.18 probably belongs to the monomer co-ordinated with a methanol molecule.

The addition of methanol induces, at the same time, two new signals farther apart; the one to high field of $g = 6$ is the more intense of the two, and appears to be a doublet with $g = 3.46$ and 3.11, respectively, whereas the other occurs at $g = 11.87$. These two signals appear to have the same origin as those observed for *meso*-nitro-octaethylporphyrinatoiron(III) in toluene with regard to locations and intensity ratios, which change as the total concentration of hemin is varied; the signal at 11.87 shows the greater decrease in intensity as the total concentration is lowered. The effect of methanol addition saturates around 20 μl cm^{-3}. Similar spectra are obtained in alkaline solutions. The total intensity remains approximately the same after the methanol addition.

The effect of adding ethanol or butanol is similar but

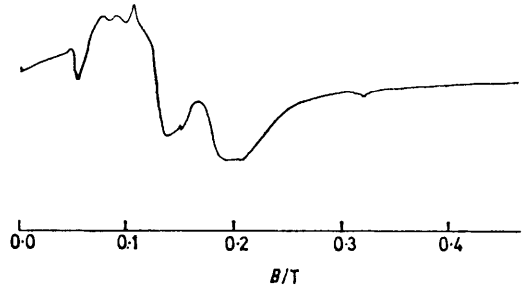

FIGURE 6 E.s.r. spectrum of hemin in aqueous alkaline solution (1×10^{-3} mol dm^{-3}, pH 11.5) with added sucrose (*ca.* 0.15 mol dm^{-3}) at 14 K

much less pronounced. The addition of ethylene glycol or sucrose gives rise to another group of signals in the $g = 8$—9 region, in addition to those due to the methanol effect. A typical spectrum is shown for the case of sucrose in Figure 6; the absorptions in the $g = 8$—9 region (0.07—0.08 T) are markedly enhanced concomitantly with the trough at $g = 4.8$ (*ca.* 0.13 T), compared to the case of methanol addition. These signals at $g = 8$—9 are observed also for hemin–methanol systems, but with much lower intensity and are not clearly discernible. Since they lose intensity when the temperature is lowered, as does the signal at $g = 4.8$, these signals may well be of the same origin.

A dimethyl sulphoxide (dmso) solution of hemin (4.83×10^{-3} mol dm^{-3}) shows a typically axial, narrow, perpendicular signal with $g = 6.0$ (measured at the peak). The doublet to higher field, which corresponds to the one observed in the alkaline methanol system ($g = 3.46$ and 3.11), can barely be seen and has a somewhat different line shape (Figure 7) from that of hemin in alkaline methanol. However, the signal which is observed to low field ($g = 11.87$, see above) in an alkaline methanol solution is absent in dmso solutions. In the mixed solvent dmso–distilled water (3 : 1 v/v) the perpendicular signal becomes even narrower, and the doublet to high field vanishes completely, demonstrating that these extra signals are strongly dependent upon the solvent composition.

According to the spectrophotometric study by Brown and Lantzke,[4] hemin in dmso is known to be completely monomeric, yet the present result shows that there is a

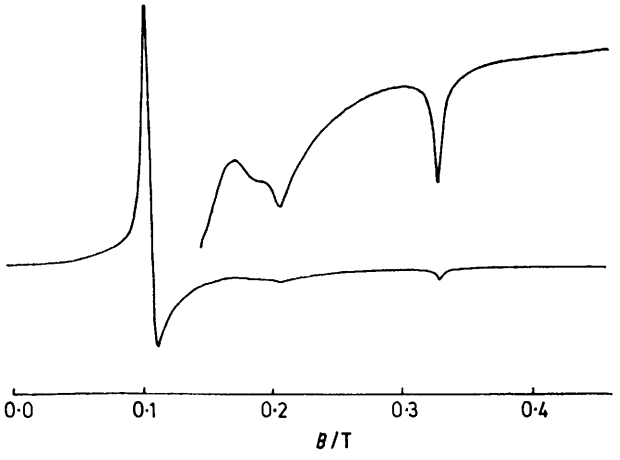

FIGURE 7 E.s.r. spectrum of hemin in dmso (4.83×10^{-3} mol dm^{-3}) at 14 K

small amount of association in the frozen state. The integrated intensity in dmso, however, is almost 2.6 times greater than that in the aqueous alkaline solution, showing that in the latter more than 60% of the hemin in solution is not seen by e.s.r.

When an increasing amount of dmso is added to an alkaline solution of hemin (pH 11.5, 9.2×10^{-4} mol dm^{-3}) a complex e.s.r. pattern develops around $g = 6$, as shown in Figure 8. The general appearance of the new absorptions

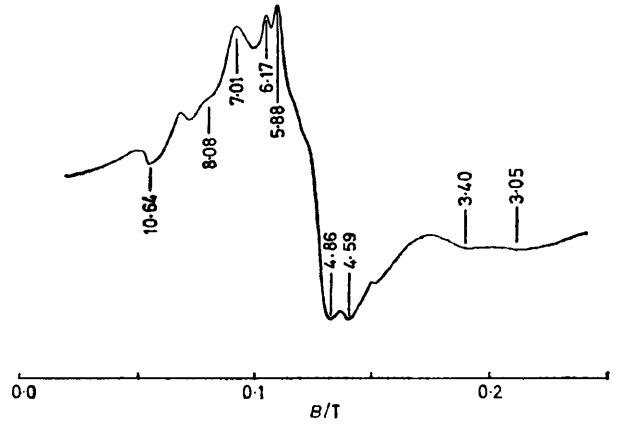

FIGURE 8 E.s.r. spectrum of hemin in aqueous alkaline solution (1×10^{-3} mol dm^{-3}, pH 11.5) with added dmso (*ca.* 1.7 mol dm^{-3}) at 14 K

is similar to that obtained by adding sucrose or ethylene glycol, except that it is better resolved in the dmso aqueous alkaline solution. The intensity of the peaks at $g = 7.03$ and 5.95 decreases also in this case as the temperature is lowered, suggesting that the nature of the transitions may be similar to those observed in the alkaline sucrose solution.

E.S.R. Spectra of Tetrasodium Phenylporphyrintetrasulphonatoferrate(III) (2) *in Aqueous Solutions.*–In an acidic medium (pH 5.8) prepared in the same manner as for hemin solutions, (2) shows a relatively broad perpendicular

absorption with axial symmetry, and weak satellites (g = 10.4 and 3.0) which are very broad and show no fine structure (Figure 9). As the pH of the solution is increased, the g = 6 signal becomes narrower but less intense, reaching a minimum at nearly neutral pH (*ca.* 6.5). In alkaline solution, the g = 6 monomer signal increases in intensity

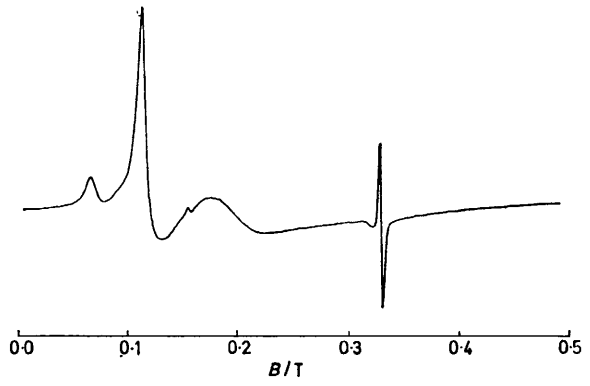

FIGURE 9 E.s.r. spectrum of (2) in aqueous solution (4.6×10^{-3} mol dm^{-3}, pH 5.8) at 14 K. The narrow free-radical signal of unknown origin in the g = 2 region is observed only at pH *ca.* 6

while keeping the narrow axial shape, but at pH 11.9 it abruptly changes to the pattern observed in an alkaline hemin solution, with a pair of shoulders roughly 0.013 T apart on both sides. The g values are 6.63, 6.08, and 4.96 (measured at the peak positions). The satellites with g *ca.* 10.3 and 3, respectively, on the other hand, decrease in intensity as the pH is raised and become undetectable in neutral solution.

Addition of methanol to a solution of (2) gives rise to a change near g = 6 and to a several-fold increase in intensity in the g = 6 region, as shown in Figure 10. However, in contrast to the case of hemin, methanol (or sucrose) addition does not induce the formation of two satellites of the type, which occur farther apart to high and low field (g *ca.* 3 and 11), respectively, in an alkaline methanol solution.

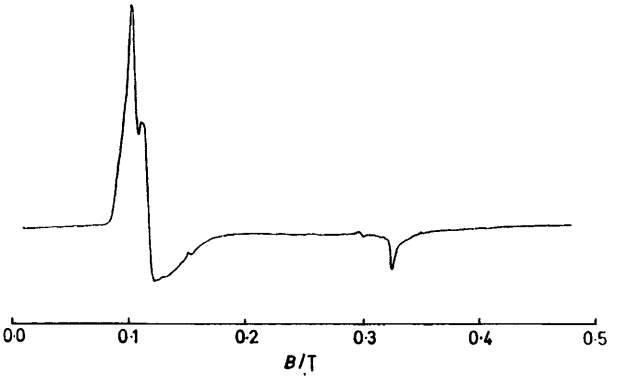

FIGURE 10 E.s.r. spectrum of (2) in aqueous alkaline solution (4.6×10^{-3} mol dm^{-3}, pH 11.7) with added methanol (0.4 : 1 v/v) at 14 K

Classification of Extra E.S.R. Signals.—The extra e.s.r. signals described above may be divided roughly into the following three types. (I) The two signals with g values around 3 and 11, respectively, which are typically observed for compound (1) as doublets, and in the neutral and alkaline aqueous solutions of hemin with added methanol, as well as in acidic aqueous solutions of (2) as broad structureless signals. The nature of the signals from the fluoride is not clearly understood. Observation of the type (I) signals seems to require some hydrophobicity in the solution. (II) A narrow absorption with g very close to 6, showing a pair of shoulders roughly 0.013 T apart from the centre. This is observed in alkaline solutions of hemin or (2). (III) The various absorptions in solutions of hemin or of (2). A complete explanation of all these signals appears at present to be a forbidding task, partly because of the lack of information other than g values. Also the requirement of frozen solutions for e.s.r. observation makes it somewhat tenuous to utilize the well documented optical data, which are obtained in liquid solutions, as the reference point for interpretation of e.s.r. data. However, there is enough evidence which strongly suggests that some of the signals observed are due to the dimeric species. For example, of the two signals of type (I), the one to high field having g = 3—4 can be attributed to some type of dimeric species. The signal intensity–concentration relations described above clearly show that the species is an association product, and the fact that this signal to high field continues to be detectable to a much lower concentration than the one to low field points to the dimer being produced in the first step of association. In the zinc(II) and copper(II) analogues of the octaethylporphyrinato-complexes, studied by n.m.r.[13–15] and e.s.r.,[22] respectively, the dimer formation and the enhancing effect of *meso*-nitro-substitution are well established. The similar trend among the iron(III) complexes shown in Figure 2 consistently supports dimerization taking place in a moderately concentrated solutions. However, when the curve-fitting of the signal intensity is made according to a simple monomer $\rightleftharpoons$ dimer scheme, using the equilibrium constant (K) and the intensity–concentration proportionality constant (C) as adjustable parameters, the parameters thus determined have considerably large standard errors and mutual dependency values close to 1.0, indicating that the simple model is inadequate for quantitative explanation of results and that a higher-order aggregation is taking place simultaneously. Nevertheless, the qualitative trend that the *meso*-nitro-substitution(s) in the porphyrin ring results in the large K value, which is one order of magnitude higher than in the unsubstituted complex, is in agreement with the case of octaethylporphyrinatocopper(II) in which π–π dimer formation is proven.

Calculation and Simulation of the Dimer E.S.R. Spectra.—In order to obtain insight into the nature of some of the observed e.s.r. transitions, theoretical calculations were made based upon the spin Hamiltonian (1) where the first

$$\mathcal{H} = D(S^2_{1z} + S^2_{2z}) - JS_1S_2 + H_{\text{Zeeman}} + H_{\text{dipole}} \quad (1)$$

two terms are the zero-field splitting of the monomers, while the second is the isotropic spin-exchange interaction. An appropriate basis set for a dimer consists of all combinations of $|I,J\rangle = |I\rangle|J\rangle$, in which $I,J = \pm\frac{1}{2}, \pm\frac{3}{2}, \pm\frac{5}{2}$ are the monomer states in the high-spin iron(III) complex. In the dipolar interaction, only those configurations are considered in which the two porphyrin planes are arranged parallel as shown in Figure 11.

In order to estimate rigorously the zero-field splitting in

$$\mathcal{H}^0 = D(S^2_{1z} + S^2_{2z}) - JS_1S_2 \quad (2)$$

the lowest energy levels due to the exchange interaction only, the truncated spin Hamiltonian (2) was solved with the complete basis set, and some of the lower energy levels

are plotted against J/D in Figure 12 as is the zero-field splitting of the lowest triplet for various D values in Figure 13. Assuming D of the monomer to be in a reasonable range, 4—8 cm^{-1}, the zero-field splitting due to the exchange

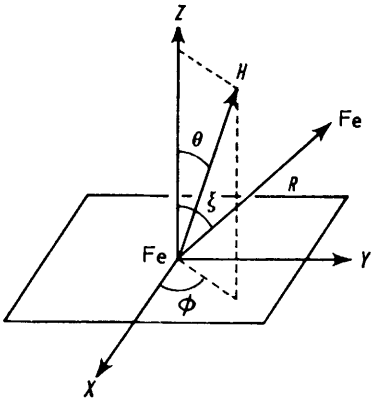

FIGURE 11 Configuration of the dimer

term is seen to exceed the microwave quantum (*ca.* 0.3 cm^{-1}) when $|J|$ is only 0.05—0.1 cm^{-1}. The dipolar interaction would also result in some zero-field splitting of the order of 0.1—0.2 cm^{-1} depending upon the structure of the dimer. The actual zero-field splitting is the sum or difference, depending upon the sign of J, of the two contributions. In any event, when $|J|$ is larger than *ca.* 0.1 cm^{-1} the only X-band e.s.r. transition to be expected is the one between the levels p and q (Figure 13, insert). Calculation also

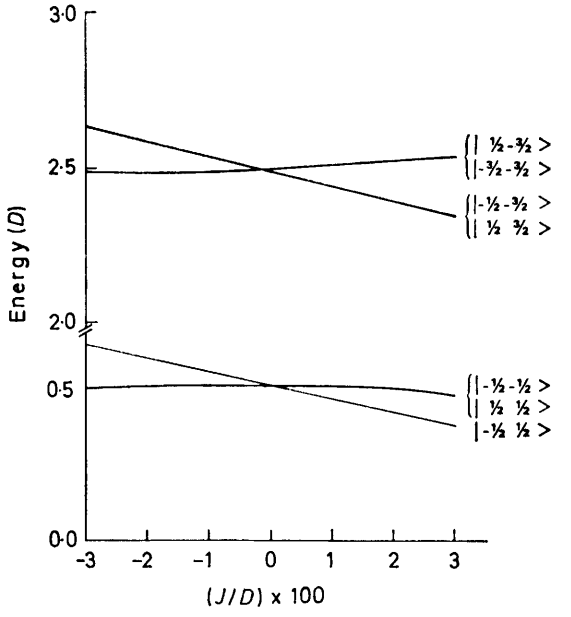

FIGURE 12 Plots of lower energy levels against J/D for the dimer with only the exchange term included. The 21 × 21 matrices with complete basis set were solved. The energies are expressed in units of the zero-field parameter D. The thin line represents the non-degenerate level, all the other levels are doubly degenerate. Only the dominant basis state of the linear combination is indicated for the lowest three levels

shows that as the zero-field splitting becomes larger the Zeeman splitting of the levels p and q becomes smaller so that eventually the transition $p \leftarrow q$ is forced toward the very high magnetic field region. Thus the fact that one e.s.r. transition is observed around 0.02 T seems to restrict $|J|$ to a rather small value.

The straightforward solution of the complete problem would require diagonalization of 21 × 21 matrices, even if the basis set were limited to symmetric combinations of the type $c(|I\rangle|J\rangle + |J\rangle|I\rangle)$, for all the variations of D and J as well as the structural parameters in the dipolar term. To make the calculation more tractable, and to obtain a qualitative description of the e.s.r. transitions to be expected, the basis set is limited to the three symmetric combinations of the lowest Kramers doublet with $I,J = \pm\frac{1}{2}$ (Figure 12). The matrix (3 × 3) for the Zeeman and dipolar term is then diagonalized. An empirical parameter (d) is added to the diagonal element of the non-degenerate level r to take account of the zero-field splitting due to the

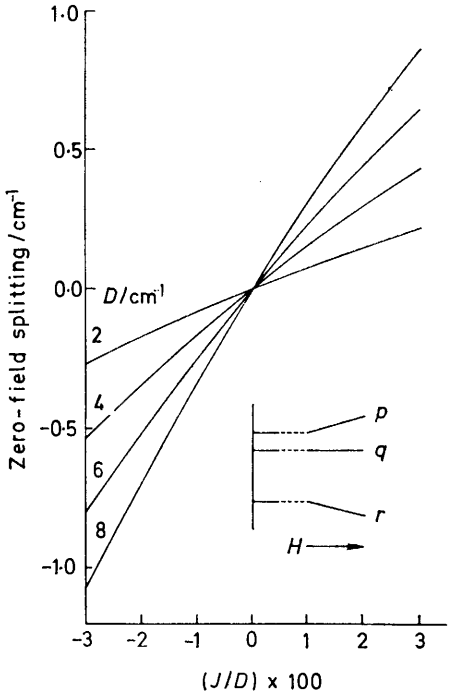

FIGURE 13 Plot of zero-field splitting against J/D for the lowest triplet levels shown in Figure 12. The energy-level designation of the lowest triplet shown as an insert is for the general case in which the dipolar interaction is included, lifting all the degeneracies in the triplet

exchange interactions, including those with the upper Kramers doublets which are ignored in this approximation. The energy levels thus obtained are shown schematically in Figure 13 (insert). The resonance diagram is calculated for the entire spatial orientation of the dimer, from which a powder pattern is calculated by a Gaussian convolution, followed by taking the first derivative.

Using this model, the high-field signal of type (I) is assigned to the transition $p \leftarrow q$ for the following reason: of the possible transitions between the three levels, this is the only one which can be made to occur in the observed magnetic field, 0.15—0.2 T, by adjusting the zero-field parameter d and the structural variables. Furthermore, the calculated powder pattern for this absorption is restricted, in agreement with the observation, to a relatively narrow region (*ca.* 0.08 T) for the entire range of molecular orientation in space. On the other hand, the transition $q \leftarrow r$ always occurs to low field of the $g = 6$ monomer peak, and

covers a much wider range of field (>0.3 T) as the molecular orientation is varied. The observed signal intensity precludes assigning it to the transition $p \leftarrow r$, since the calculated transition probability is too small.

Typical resonance diagrams of the transition $p \leftarrow q$ for three arbitrarily chosen sets of structural parameters are shown in Figure 14. The observed powder pattern shows a

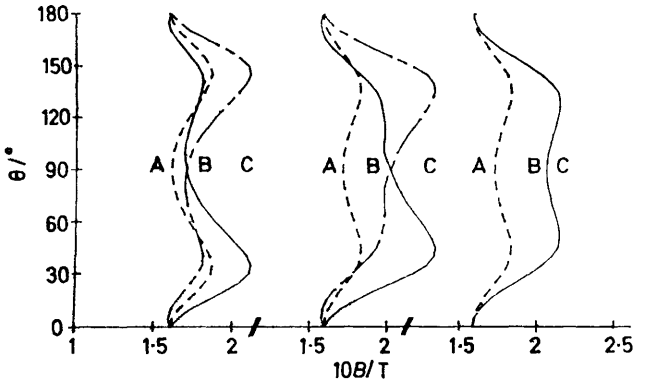

FIGURE 14 Resonance diagram for the transition $p \leftarrow q$. $\phi = 0$ (——), 90 (– – –), or 180° (— – —); Left: R(Fe–Fe) =3.7 Å, $\xi = 10°$, and $d = 0.6$ cm^{-1}, where d is an adjustable parameter to account for the zero-field splittings due to exchange interactions. A positive d lowers the non-degenerate level and corresponds to the ferromagnetic coupling. Centre: R(Fe–Fe) = 4 Å, $\xi = 20°$, and $d = 0.75$ cm^{-1}. Right: R(Fe–Fe) = 4 Å, $\xi = 0°$, $d = 0.8$ cm^{-1}, and $e = -0.023$ cm^{-1}, where e is an adjustable parameter added to the non-diagonal element connecting the p and q levels (Figure 13, insert)

doublet structure [except in the case of (2), each component having almost equal intensity (see, for example, Figure 1, signal D)]. The low-field component crosses the baseline, while the high-field component is bell-shaped, indicating that the former corresponds to the peak in the absorption curve and the latter to a shoulder. This is an indication of some anisotropy in the dimer structure, and may be explained by the presence of two or more extrema in the resonance diagram, such as those indicated in Figure 14 (A, B, C). In spectral simulation, based upon the resonance diagram, the two components may be elicited in various ways; for example, in Figure 14 (left), in which a relatively small skew angle ξ is assumed, the extrema A and B occur near $\theta = 90°$ and C at 30°, respectively. The two observed components are assigned, respectively, to the extremum C and to A,B combined. (In the limiting case of $\xi = 0$, these correspond, respectively, to the so-called perpendicular and parallel peaks.) However, C does not give rise to as much relative intensity in the calculated spectrum as is actually observed. Alternately, in Figure 14 (centre), the components are fitted to the extrema A and B, respectively, by assuming a more skewed dimer structure (*i.e.* a large ξ), but, then, the extremum C causes an additional peak, although with low intensity, in the simulated spectrum, in contrast to the observed spectrum. If an antiferromagnetic exchange interaction is assumed (*i.e.* a negative d value) as well as a large ξ, a two-component spectrum can be obtained, but with the location of the peak and shoulder interchanged. The only way to reproduce a correct two-component powder pattern is to introduce an empirical additive parameter e to the off-diagonal elements of the 3 × 3 matrix and to set the skew angle ξ equal to zero. This is equivalent to adding a rhombic term to the original spin Hamiltonian (1), and causes a similar in-plane anisotropy, as does a skewed structure. The resonance diagram for this case is shown in Figure 14 (right), and the resulting powder pattern in Figure 15(*a*), which is in reasonable agreement with the observed spectrum with respect to its location and the magnitude of the doublet splitting. It is to be noted that R and d cannot be uniquely determined. Other signals of the type (I) (*e.g.* that observed with hemin in alkaline methanol solution) can be simulated by adjusting d, e, and the Gaussian linewidth in convolution.

The source of the smaller doublet (*g ca.* 10—11) to lower field of the monomer signal is unknown, and if it is indeed due to a higher-order association product, as suggested above, it is beyond the scope of the present formulation.

The signal of type (II) can also be simulated using the same formulations. It may be viewed as the superposition of the two closely located dimer absorptions and a

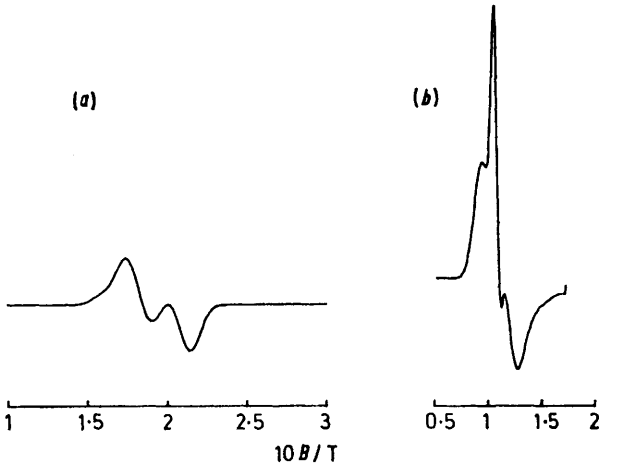

FIGURE 15 Simulated powder patterns. (*a*) A simulation for the type (I) high-field signal of (1), obtained from the diagram shown in Figure 14 (right). Resonance curves were calculated for every 5° of the polar (θ) and azimuthal (ϕ) angle. A histogram was made for the magnetic field interval (ΔH) of 0.002 T; the Gaussian linewidth (standard deviation) used for convolution = 0.006 T. (*b*) A simulation of the type (II) signal. Resonance curves were calculated for every 2° of θ and ϕ, histogram interval (ΔH) = 0.001 T, and Gaussian linewidth =0.007 T for the dimer, 0.003 T for the monomer

sharp monomer peak in the middle. In order for the dimer transitions $p \leftarrow q$ and $q \leftarrow r$ to occur near the monomer peak, the zero-field splitting must be very small. In the simulation, the zero-field parameter d for exchange interaction is set equal to zero. A Fe–Fe distance of 7.2 Å and a large skew angle of 60° are assumed. The calculated spectrum is qualitatively in agreement with the observed type (II) signal [Figure 15(*b*)]. As far as the perpendicular absorption is concerned, a similar result can be obtained with the zero skew angle. However, the calculation predicts that with $\xi = 0$ the parallel absorptions due to the dimer should occur at *ca.* 0.025 T on both sides of the $g = 2$ parallel peak of the monomer, whereas no such signals have actually been detected. With a large skew angle $\xi = 60°$, on the other hand, the separation of the two is calculated to be only *ca.* 0.008 T, well within the linewidth of the observed $g = 2$ signal.

DISCUSSION

The nature of the interaction in the dimer, which gives rise to the signal D, is probably of the π–π type, in which

the electronic polarization between the metal and the π system has a dominant role. This is indicated by the remarkable increase in signal intensity as a result of *meso*-substitution of a strongly electron-withdrawing nitro-group. A similar situation was observed for copper(II) analogues in which a dimer structure having the two porphyrin planes arranged parallel to each other has been determined by e.s.r. study.[22] In the present case, the two Fe–Cl bonds may be either pointing outwards or sandwiched between the porphyrin planes. The latter arrangement has an advantage in providing a mechanism for the rhombicity in the ligand field around the iron(III) ions. The possibility of having hydroxide groups in place of Cl^- (namely, a dihydroxo-bridged structure) is completely ruled out in the case of the halogeno(*meso*-nitro-octaethylporphyrinato)iron(III) complexes in toluene on the grounds that no difference was observed between two experiments, one conducted using carefully dried materials in a vacuum system, and the other in which a small amount of water was deliberately added to the solution. In aqueous systems, this possibility may exist. However, the magnitude of the exchange interaction estimated for other dihydroxo-bridged dimers (-8 cm^{-1}) [21] is too large to explain signal D in the above formulation, provided that the estimated J value would indeed apply to iron(III) porphyrins.

The assignment made above for the type (II) signal, a sharp peak with $g = 6$, and the shoulders, to a transition in a dimer having a large Fe–Fe distance and a skew angle seems to explain the spectral characteristics satisfactorily. The condition in which this type of signal is obtained always requires OH^-, which may act as a bridging unit by itself or, with another component. A variety of such schemes for dimeric intermediates involving OH^- has been discussed by Sadasivan *et al.*[5] In any event, if the signal does represent a dimer, the structure must be the one in which the exchange interaction is very small so that the two rhombic absorptions appear almost superimposed on each other and on the monomer peak. This type of signal has also been observed in *meso*-tetra(4-carboxyphenyl)porphyrinato-iron(III) complexes at pH 12.4 by Stong and Hartzel,[27] who assigned it to the oxo-bridged dimer transition on the basis of the spectrophotometric and e.s.r. pH titrations. The interpretation, however, appears to be in conflict with the fact that an e.s.r. signal is absent in the known μ-oxo-dimer [9] in which the two iron(III) ions are antiferromagnetically coupled to give a diamagnetic ground state with some paramagnetic contribution from the nearby excited states.[28]

Previously, it was deduced from spectrophotometric studies at room temperature that chlorohemin in an alkaline solution is almost completely dimerized,[4] and the μ-oxo-dimer was proposed to explain the results. However, the magnetic susceptibility, measured also at room temperature,[10] is shown to be only slightly lower (the effective magnetic moment *ca.* 5.5 B.M.*) than the value expected for the high-spin monomer (5.9 B.M.), and certainly much higher than predicted if the hemin is completely converted into the μ-oxo-dimer. Although the spectrophotometric measurements were made in the presence of electrolytes, which are known to result in low susceptibility species (see below), the buffer concentration was not high enough to explain the discrepancy. It thus follows that most of the dimeric species existing in the alkaline solution have a magnetic moment per iron(III) ion almost as high as that of the high-spin monomer, or that the magnetic property of the monomer units in the dimer is not greatly perturbed by the dimer formation. Our e.s.r. observation indeed shows that *ca.* 40% of the total concentration is represented by the type (II) signal, which occurs superimposed upon the $g = 6$ monomer signal, indicating the close similarity of their magnetic properties. The large Fe–Fe distance and skew angle which are needed to simulate the signal on the basis of the dimer are consistent with this interpretation.

The rest of the molecular species which are not observed by e.s.r. may be in the form of (*a*) the μ-oxo-dimer, (*b*) other dimeric species having large zero-field splittings, or (*c*) various aggregates. Undoubtedly, freezing the solution for e.s.r. observation would promote the formation of such species, which are expected to have substantially lower magnetic susceptibilities.[10]

The effect of NaCl in reducing the signal intensity is in accordance with the magnetic susceptibility,[10] and strongly suggests that the species represented by the type (II) signal is a precursor of the low-susceptibility species. The two iron(III) porphyrin molecules which are held at an appreciable distance due to electrostatic repulsion may be brought into closer contact as a result of charge neutralization (or shielding) by the added electrolyte. This will facilitate μ-oxo-dimer formation, or closer aggregation.

Addition of methanol apparently rearranges the dimer structure, which is represented by the type (II) signal, in favour of the π–π type association, probably by virtue of the hydrophobic environment. Adding ethylene glycol or sucrose clearly increases the overall signal intensity, although quantitative estimation is made difficult by the absorption which extends to zero magnetic field. These reagents may be deaggregating [10] the low-susceptibility species mentioned above to form species of smaller size which show the e.s.r. absorptions. The observed π–π type signal may indeed be a result of such deaggregation. The complex signals near $g = 6$ observed on sucrose addition represent more than one species, some of which may be due to antiferromagnetically coupled species, since some of the signals disappear on lowering the temperature.

The water-soluble complex (2) has been shown to be monomeric in acidic solutions and to exist as the μ-oxo-bridged dimer in alkaline media.[6,8] The e.s.r. result shows that in a frozen solution there is slight formation of the π–π-type dimer, which diminishes upon increasing pH, most likely due to the increase in the net charge of the monomer. Above pH 11, the type (II) signal

* Throughout this paper: 1 B.M. ≈ 9.27×10^{-24} A m^2.

appears, suggesting that a distant dimer similar to that of hemin is formed.

In summary, the present e.s.r. study shows that while the formation of the μ-oxo-bridged dimer may indeed take place, as has been almost exclusively assumed to be the case when dimerization is demonstrated, there are other species which should be taken into account. For example, we have shown that π–π-type dimers are formed in organic solvents and even in aqueous solutions where a hydrophobic environment is provided, and that another type of dimer having a large Fe–Fe distance and skew angle may exist in alkaline solutions. There are evidently aggregations as well as other possible dimeric species, some of which are detected by e.s.r. by the signal around $g = 8$—9. Change of solvent composition and pH then appears to interconvert one type to another as described above.

The authors are indebted to W. H. Jennings and G. Knott for their help in using the MLAB and graphics facilities. Partial support (to K. M. S.) of this work by the National Institutes of Health (HL 22252) is gratefully acknowledged.

[9/744 *Received*, 14*th May*, 1979]

REFERENCES

[1] J. E. Falk, ' Porphyrins and Metalloporphyrins,' Elsevier, Amsterdam, 1964; H. Scheer and J. J. Katz, ' Porphyrins and Metalloporphyrins,' ed. K. M. Smith, Elsevier, Amsterdam, 1975, pp. 399—524, and refs. therein.

[2] Y. Inada and K. Shibata, *Biochem. Biophys. Res. Comm.*, 1962, **9**, 323.

[3] D. W. Urry and J. W. Pettegrew, *J. Amer. Chem. Soc.*, 1967, **89**, 5276; D. W. Urry, *ibid.*, p. 4190.

[4] S. B. Brown and I. R. Lantzke, *Biochem. J.*, 1969, **115**, 279; S. B. Brown, T. C. Dean, and P. Jones, *ibid.*, 1970, **117**, 733.

[5] N. Sadasivan, H. I. Eberspaecher, W. H. Fuchsman, and W. S. Caughey, *Biochemistry*, 1969, **8**, 534.

[6] E. B. Fleischer, J. M. Palmer, T. W. Srivastava, and A. Chatterjee, *J. Amer. Chem. Soc.*, 1971, **93**, 3162.

[7] H. Goff and L. O. Morgan, *Inorg. Chem.*, 1976, **15**, 2062.

[8] J. R. Sutter, P. Hambright, P. B. Chock, and M. Krishnamurthy, *Inorg. Chem.*, 1974, **13**, 2764.

[9] K. M. Kadish, G. Larson, D. Laxa, and M. Momenteau, *J. Amer. Chem. Soc.*, 1975, **97**, 282.

[10] G. Blauer and A. Ehrenberg, *Biochim. Biophys. Acta*, 1966, **112**, 496.

[11] I. A. Cohen, *J. Amer. Chem. Soc.*, 1969, **91**, 1980.

[12] A. M. T. Jehanli, D. A. Stotter, and M. T. Wilson, *European J. Biochem.*, 1976, **71**, 613.

[13] R. J. Abraham, F. Eivazi, H. Pearson, and K. M. Smith, *J.C.S. Chem. Comm.*, 1976, 699.

[14] R. J. Abraham, G. H. Barnett, G. E. Hawkes, and K. M. Smith, *Tetrahedron*, 1976, **32**, 2949.

[15] R. J. Abraham, B. Evans, and K. M. Smith, *Tetrahedron*, 1978, **34**, 1213.

[16] G. N. La Mar and D. B. Viscio, *J. Amer. Chem. Soc.*, 1974, **96**, 7354.

[17] R. V. Snyder and G. N. La Mar, *J. Amer. Chem. Soc.*, 1977, **99**, 7178.

[18] J. Shack and W. M. Clark, *J. Biol. Chem.*, 1949, **171**, 143.

[19] E. B. Fleischer and T. S. Srivastava, *J. Amer. Chem. Soc.*, 1969, **91**, 2403.

[20] H. Schugar, C. Walling, R. B. Jones, and H. B. Gray, *J. Amer. Chem. Soc.*, 1967, **89**, 3712.

[21] H. J. Schugar, G. R. Rossman, and H. B. Gray, *J. Amer. Chem. Soc.*, 1969, **91**, 4564.

[22] M. Chikira, H. Kon, R. A. Hawley, and K. M. Smith, *J.C.S. Dalton*, 1979, 245.

[23] B. Evans, and K. M. Smith, *Tetrahedron Letters*, 1977, 3079; B. Evans, K. M. Smith, and J. A. S. Cavaleiro, *J.C.S. Perkin I*, 1978, 768.

[24] J.-H. Furhop and K. M. Smith, ' Porphyrins and Metalloporphyrins,' ed. K. M. Smith, Elsevier, Amsterdam, 1975, p. 800.

[25] G. Knott, ' Modeling, Computation and Graphics,' Division of Computer Research and Technology, National Institutes of Health, Bethesda, 1977.

[26] M. Chikira, H. Kon, and K. M. Smith, *J.C.S. Chem. Comm.*, 1978, 906.

[27] J. D. Stong and C. R. Hartzel, *Bioinorg. Chem.*, 1976, **5**, 219.

[28] A. Earnshaw, ' Introduction to Magnetochemistry,' Academic Press, London, 1968, ch. 5.